3D-hydromechanical Behavior of a Stimulated Fractured Rock Mass

Xavier Rachez, Sylvie Gentier

3D-hydromechanical Behavior of a Stimulated Fractured Rock Mass

Xavier Rachez and Sylvie Gentier

BRGM, Geothermal Department, 3 Av. Claude Guillemin, BP 36009, Orléans - France

x.rachez@brgm.fr

Keywords: Fractured reservoir, hydro-mechanical modelling, hydraulic stimulation, Soultz-sous-Forêts

ABSTRACT

The EGS concept has the necessity to increase the local natural permeability of low permeability rock masses. Hydraulic stimulation is a widely used technique to increase the permeability. This technique was applied at various depths in the wells of the Soultz-sous-Forêts site since the beginning of the project. This has yielded an effective and irreversible increase in permeability, which is associated with microseismic events. The understanding of the mechanisms that lead to local increases in permeability is essential to the development of this technique.

Based on all the hydraulic stimulation tests that have been performed in the wells, a 3D hydro-mechanical model is proposed. The fracturation model selected around each well contains large deterministic fault zones (hectometric size), since they likely connect the well to the reservoir and potentially react during the hydraulic stimulation tests.

A 3D Distinct Element Method model was developed, with a specific hydro-mechanical coupling, where flow takes place only in the fractures and the rock matrix is impermeable and deformable. The constitutive law of the fault zones is a Mohr-Coulomb law for the mechanical part with an independent associated dilatancy law for the hydraulic part. Hydraulic stimulation tests and post-stimulation injection tests have been performed with this model. The results obtained clearly indicate how an irreversible increase in the permeability is caused by the shearing that occurs in the fault zones during the hydraulic stimulation tests. The location of this shearing in the fault zones results from the combination of the in-situ stresses, their orientations, and their interconnections. The magnitudes of the calculated shear displacements were found to be consistent with the observations along the wells and the information obtained from the analysis of the microseismic events.

1. INTRODUCTION

Experiments were initiated at the Soultz-sous-Forêts site (France) in 1987 with the goal to produce electricity from the heat available in the granite basement. To do so, three boreholes (GPK2, GPK3 and GPK4) were drilled down to 5 km depths. Heat is extracted from this geothermal borehole triplet by injecting fresh fluid in one of the three wells (the injection well, GPK3) and by pumping some hot fluid in the two other wells (the production wells, GPK2 and GPK4). For such a system, the heat extraction efficiency depends on the flow pathways within the pre-existing fractures and on the fluid velocities between the injection wells and the production wells. This efficiency is the key parameter that determines whether the exploitation of a geothermal reservoir is economically viable: the energy produced with the extracted heat must exceed the energy needed for extracting heat. As the granite massif at a 5 km depth has a

very low permeability, the heat extraction is efficient only if the permeability is successfully increased.

Many experiments have been conducted at the Soutz-sous-Forêts site, including hydraulic stimulations of the wells. These hydraulic stimulations have increased the permeability of the rock mass in the vicinity of the wells. This permeability increase is irreversible so that, after the hydraulic stimulation, it is possible to inject higher flowrates for small pressure increases (Gérard et al., 2000). Understanding the mechanisms that take place during a hydraulic stimulation is a key issue in the optimization of the heat extraction efficiency of an EGS reservoir.

Thermo, hydraulic, and mechanical effects take place during a hydraulic stimulation. In this paper, only the hydro and mechanical effects are studied. Those effects depend mostly on the fractures, their interconnections, their hydro-mechanical features, and the relationship between their orientation and the in-situ stress state. The adopted numerical approach successfully simulated hydro-mechanical processes due to fluid flows in deformable joints. The modelling approach was first applied to the shallow reservoir (Gentier et al., 2004) and was later enhanced when applied to the deeper reservoir (Gentier et al., 2005, Rachez et al., 2006). The results obtained clearly indicate how increases in permeability are caused by the shearing that occurs in the fault zone during the hydraulic stimulation tests, and how the orientation of the most permeable fractures is related to the orientation of the in-situ stresses. Recent new enhancements such as the modelling of a well shutdown were used to simulate stimulation tests followed by post-stimulation injection tests (Gentier et al., 2008). This paper presents the modelling of the hydraulic stimulation test and the post-stimulation injection test performed in GPK4, which shows that the permeability increase created by the hydraulic stimulation test is irreversible and is caused by the shearing of the fault zone planes.

2. CONSTRUCTION OF THE NUMERICAL MODEL

2.1 Short Description of the Numerical Approach

In order to simulate the behavior of the fractured rock mass in the vicinity of the wells during their hydraulic stimulations, the numerical approach must take into account the fractures and the hydro-mechanical coupling between the fluid within the fractures and the rock mass. Numerical approaches such as the Finite Elements Method are not well suited as they are limited in their consideration of complex fractured rock masses. Therefore, a 3D Distinct Element Method code was used (3DEC, 2008), which was adapted to take into account such fractured systems.

Initially devoted to the modelling of three dimensional mechanical problems, the code has been extended within the frame of research projects funded by the French Agency for Energy and Environment (ADEME) in order to simulate hydro-mechanical processes due to fluid flows in

deformable joints, as well as thermo-hydro-mechanical processes.

Thus, it allows the simulation of interactions between the mechanical (deformations, stresses, etc.) and hydraulic processes (pressures, apertures, etc.) in a rock mass cut by discrete discontinuities that correspond to a realistic geometry of the fracture network. The resulting blocks are considered to be deformable but impermeable. Indeed, the fluid flow occurs only in the joints, and there is no porous flow in the rock matrix. The fluid flow is laminar (obeying a cubic law) and monophasic in that the joints are either fully saturated or totally dry. This assumption is considered to be true for the Soultz-sous-Forêts granite, as the matrix permeability is negligible.

From a mechanical point of view, the behavior of the discontinuities is assumed to be elasto-plastic (see § 2.4); the blocks are deformable and are assumed to display an elastic behavior.

Concerning the numerical aspects, the blocks are discretized into tetrahedral elements and the fractures are discretized into elementary domains. The numerical resolution of the transient flows is performed by using a finite difference scheme. At each time step, the flows between nets induced by the pressure field are calculated. At constant time, the excess (or loss) of fluid volume in each elementary domain is modified by running mechanical cycles during which the fluid pressure is modified proportionally to the "non-equilibrated" volume. The modification of the pressure field results in a modification of the actual stresses applied to the surrounding formations, which may themselves cause changes in the openings of the fractures and hence of the pressure field. Since the adopted calculation method is incremental with preset time steps, equilibrium is assumed to occur in the model when the pressure and stress fields no longer change between two consecutive time steps.

The mechanical deformations in the normal direction (U_n) and hydraulic apertures (a) are related by the expression below in which a_0 represents the initial hydraulic aperture defined for each fracture:

$$a = a_0 * U_n \qquad (1)$$

2.2 Model Geometry

The numerical model is represented by a 400m*400m*1000m parallelepiped volume centered on the GPK4 open hole, whose trajectory is considered vertical. A fracture network has been defined essentially by comparing the thermal anomalies issued from the temperature log (July 2004) with the UBI (Gentier et al, 2005). Nine fault zones have been selected and introduced in the model. The fault zone geometry is detailed in **Error! Reference source not found.**. The fault zones are roughly sub-vertical and parallel to the direction of maximum horizontal stress (see § 2.3). The model is vertically centered on the F6 fault zone at a 4797 m depth.

Table 1: GPK4 – geometry of the fault zones

Fault denomination	Plane direction [°]	Dip [°]	Dip direction	Depth [m]
F1	4	86	NW	-4553
F2	11	83	NW	-4651
F3	2	80	SW	-4698
F4	167	85	SW	-4735
F5	165	75	NE	-4774
F6	147	66	NE	-4797
F7	165	69	SW	-4824
F8	173	70	NW	-4858
F9	20	78	NW	-4959

2.3 Initial and Boundary Hydro-Mechanical Conditions

The following stress field determined by Cornet et al. (2007) is considered:

$$\sigma_h = (0.54 \pm 0.02) * \sigma_v \qquad (2)$$

$$\sigma_H = (0.95 \pm 0.05) * \sigma_v, \text{ oriented N175°E +/66° } (3)$$

$$\sigma_v = \sigma_{v0} + 0.0255[MPa/m]*(depth[m]-1377) \qquad (4)$$

with $\sigma_{v0} = 1377*0.024[MPa]$

where σ_h and σ_H are the minimal and maximal horizontal principal stress, respectively, and σ_v the vertical principal stress. The direction of the maximal horizontal principal stress σ_H is N175°E $\pm$ 6°.

The distribution of the initial fluid pressure in the fractured network is assumed to behave like a hydrostatic field, as indicated in the equation below:

$$P = \rho * g * y \qquad (5)$$

where ρ, g and y are the density of water, gravity and depth, respectively. An illustration of the model showing its boundary conditions is given in Figure 1.
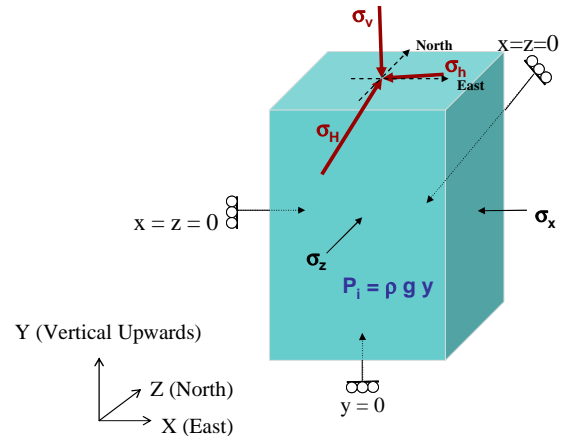

Figure 1: Initial and boundary hydro-mechanical conditions assumed in the model

The hydro-mechanical boundary conditions shown Figure 1 are the following:

- Zero displacements are imposed at the North, West and bottom faces.

- Stresses are applied on the South, East and top faces.

- The hydrostatic pressure is fixed on each face of the parallelipepided model.

2.4 Hydro-Mechanical Behavior of Fault Zones and Blocks

All fault zones have the same mechanical constitutive law. The normal mechanical behavior is elastic linear, while the fault zone is in compression, and tensile strength is null. The tangential mechanical behavior is elasto-plastic. It follows a Mohr Coulomb failure criterion with dilation effects. The shear strength of the joint is given by Equation 6:

$$\tau_s \leq c + \sigma_n * \tan \varphi \tag{6}$$

where c, σ_n and φ are the joint cohesion, the normal stress applied on the joint, and the joint friction angle, respectively.

The effects of dilation appear as soon as the maximum shear strength is reached. When the joint is slipping, the walls joint normal displacement $\Delta U_{n\text{-dil}}$ increases due to the dilation and is governed by Equation 7:

$$\Delta U_{n\_dil} = \Delta U_s * \tan \psi \tag{7}$$

where ΔU and ψ are the tangential displacement increment and the dilation angle, respectively.

In order to avoid an infinite opening of the joint when shear displacements are great, the dilation effect is stopped as soon as the tangential displacement reaches a threshold called Z_dil. The shear behavior is illustrated in Figure 2 in the case of a null cohesion.
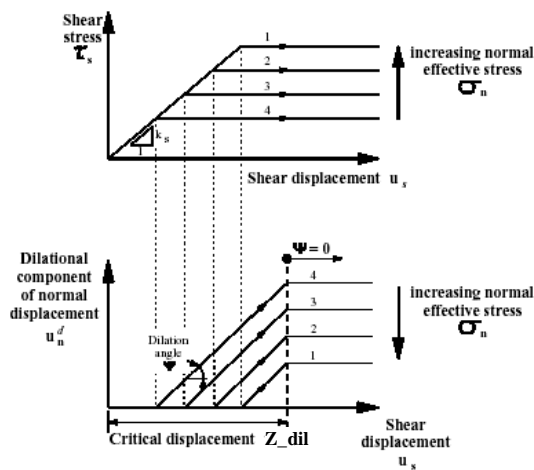

Figure 2: Illustration of the Mohr-Coulomb model with dilation effects (for a null cohesion) (3DEC, 2008)

The fault zones hydro-mechanical parameters are detailed in

Table 2 and 3.

Table 2: Fault zones mechanical properties

Kn [MPa/m]	Ks [MPa/m]	Cohesion [MPa]	Friction angle	Dilation angle	Z_dil [mm]
80 000	80 000	0	45°	1°	10

Table 3: GPK4 – Fault zones hydraulic properties

Initial aperture a_0 [mm]	Residual aperture ares [mm]	Maximum aperture amax [mm]
2.5e-3	2.5e-3	0.15

The blocks are considered to be elastic with the mechanical properties given in Table 4.

Table 4: Block mechanical properties

Density [kg/m^3]	Young Modulus (MPa)	Poisson's ratio ν
2 680	52 000	0.29

2.5 Hydro-Mechanical Coupling for Modelling a Hydraulic Stimulation Test

A Hydro-Mechanical coupling was specifically adapted in order to solve hydraulic stimulation tests and avoid potential numerical instability. This consists of alternately performing only mechanical steps and only hydraulic steps, where the numbers of mechanical and hydraulic steps are optimized using a macro language, depending on the behavior of the fractured rock mass. The run is stopped when equilibrium is reached between the injected flowrate in the well and the flowrate at the other boundary limits.

The simulation of the stimulation test is carried out in the model by adding an overpressure (ΔP) (a pressure over the hydrostatic pressure) in the open hole. In order to avoid any potential numerical instability, intermediate overpressure stages are applied instead of the two real in-situ overpressure stages that were applied in-situ. The over-pressure stages applied in GPK4 are the following (in MPa): 3.0, 6.0, 9.0, 13.75, 15.5 and 18.3 (13.75 and 18.3 being the reference overpressure values issued from the in-situ measurement in the wells).

3. RESULTS

3.1 GPK4 Hydraulic Stimulation Test

A plot of the pressure applied in the open hole versus the flowrate injected in each fault zone is shown in Figure 3. The shapes of the curves are slightly different for each fault zone, showing that their response to the hydraulic stimulation is not exactly the same. For the 13.75 MPa overpressure stage, the injected flowrate in each fault zone varied from 1.5 to 2.5 l/s. The maximum injected flowrate per fault zone is about 2.5 l/s and concerns fault zones #6, #8, #7, #2 and #5, which respectively strike N147°E, N173°E, N165°E, N11°E, and N165°E. Except for fault zone #6, whose plane direction is N147°E, the directions of the most permeable fault zones are roughly parallel to the direction of maximum horizontal stress.
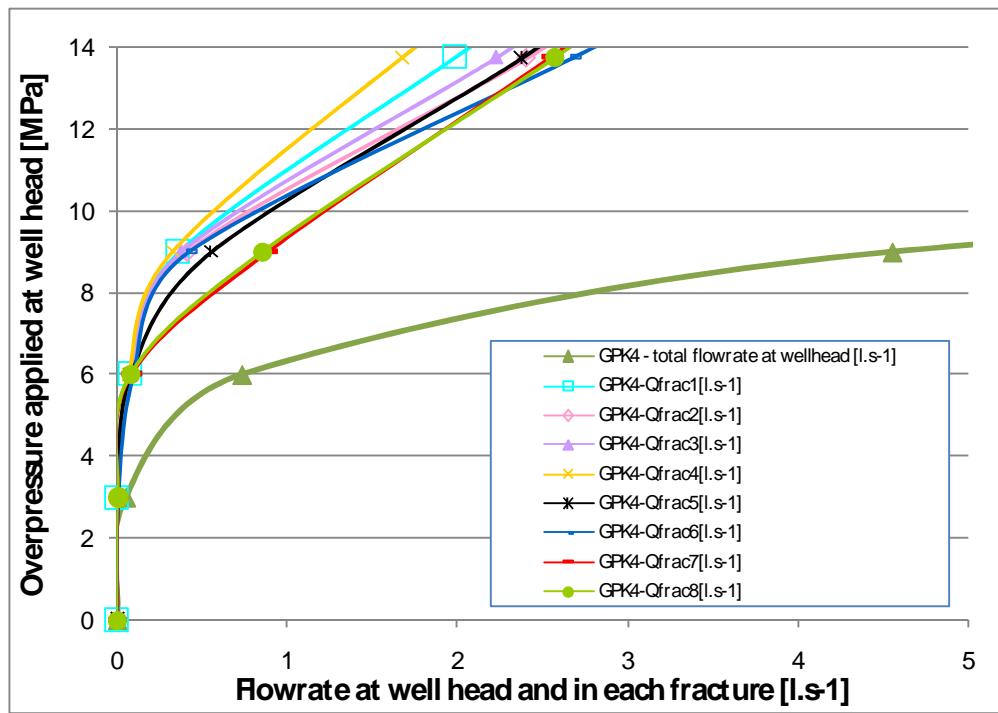
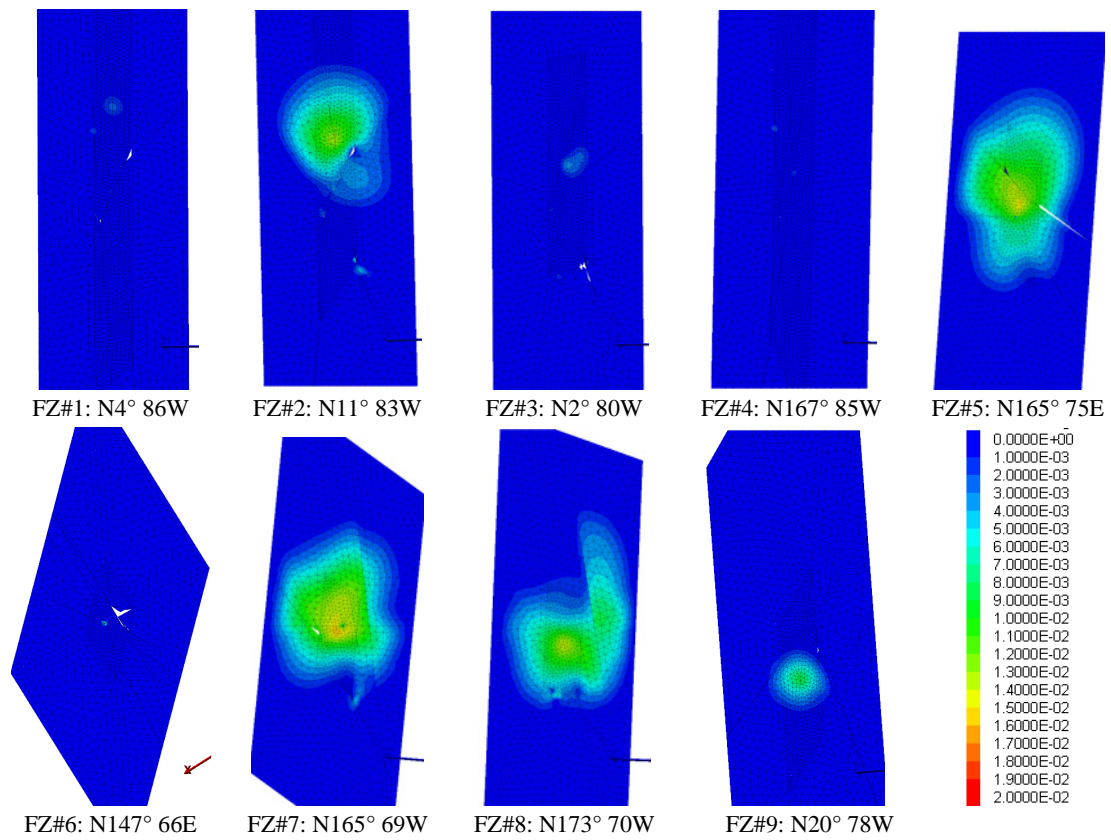Figure 3: GPK4 - Pressure vs. Flowrate calculated in each fault zone

FZ#1: N4° 86W   FZ#2: N11° 83W   FZ#3: N2° 80W   FZ#4: N167° 85W   FZ#5: N165° 75E

FZ#6: N147° 66E   FZ#7: N165° 69W   FZ#8: N173° 70W   FZ#9: N20° 78W

Figure 4: GPK4 - Shear displacement contours [m] in fault zones planes at overpressure stage ΔP = 13.75 MPa

FZ#1: N4° 86W   FZ#2: N11° 83W   FZ#3: N2° 80W   FZ#4: N167° 85W   FZ#5: N165° 75E

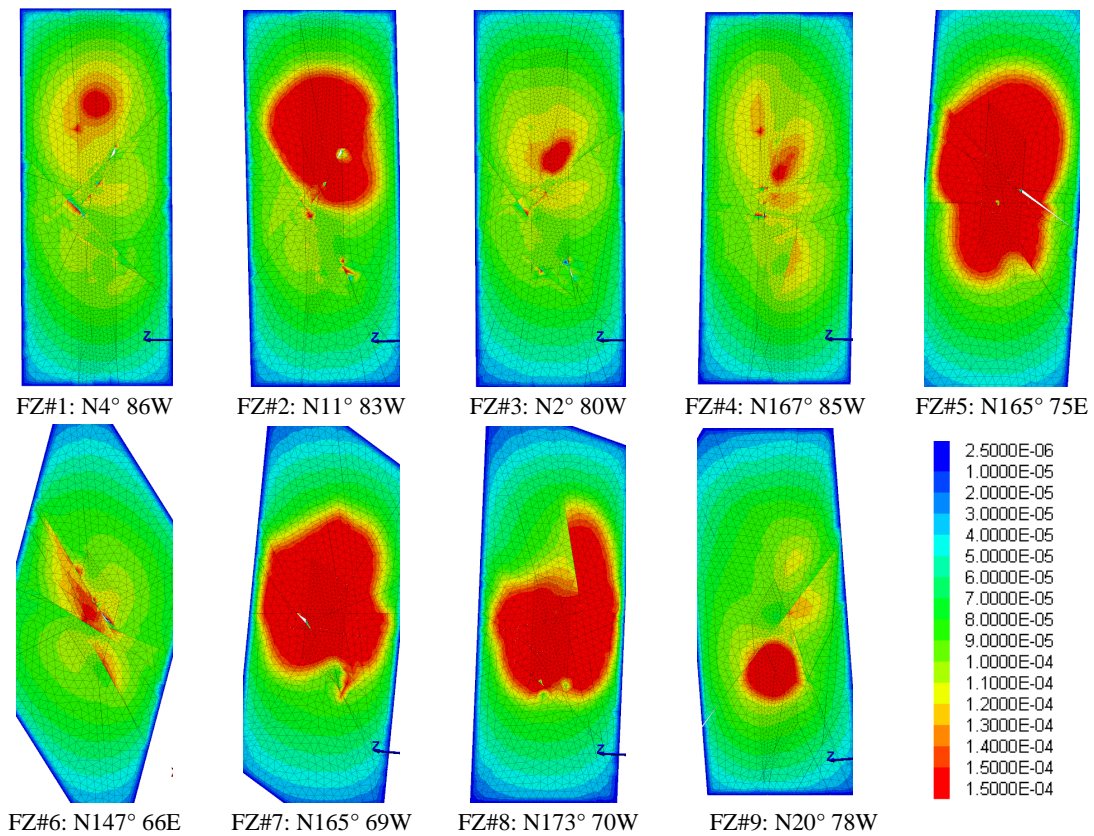FZ#6: N147° 66E   FZ#7: N165° 69W   FZ#8: N173° 70W   FZ#9: N20° 78W

Figure 5: GPK4 – Hydraulic aperture contours [m] in fault zones planes at overpressure stage ΔP = 13.75 MPa

Figure 4 and 5 respectively display the shear displacements contours and the hydraulic aperture contours obtained in each of the nine fault zone planes that cross the GPK4 open hole, for the 13.75 MPa overpressure stage.

For this overpressure stage, the most permeable fault zones are the fault zones that have the most shearing compared to the other fault zones. The maximum shear displacement is about 1.5 cm. The most permeable fault zones exhibit greater areas where the hydraulic aperture has reached the maximum hydraulic aperture allowed in the model (0.15mm).

The shape of the hydraulic aperture obtained in fault zone #6, striking N147°E, indicates that the major injected flowrate in this fault zone is due to the intersection of this fault zone with the other fault zones.

The shear displacement contours and the hydraulic contours in fault zone plane #8 for each overpressure stage applied during the stimulation test are shown in Figures 6 and 7, respectively. While the pressure applied at the wellhead increases slightly, the hydraulic aperture in the fault zone increases without any shear displacement. The fault zone simply opens itself. For the 9 MPa overpressure stage, the center of the fault zone has reached the maximum hydraulic aperture that is allowed. The shear displacement is still less than 1 mm. For the 13.75 MPa overpressure stage, a rapid increase of the hydraulic aperture was observed, which correlates to the shearing within the fault zone plane. Fault zone #8 also connects to zone #7, and the fluid flows within it. For greater overpressure stages, the hydraulic aperture somehow remains the same and the shear displacements increase up to 2 cm.
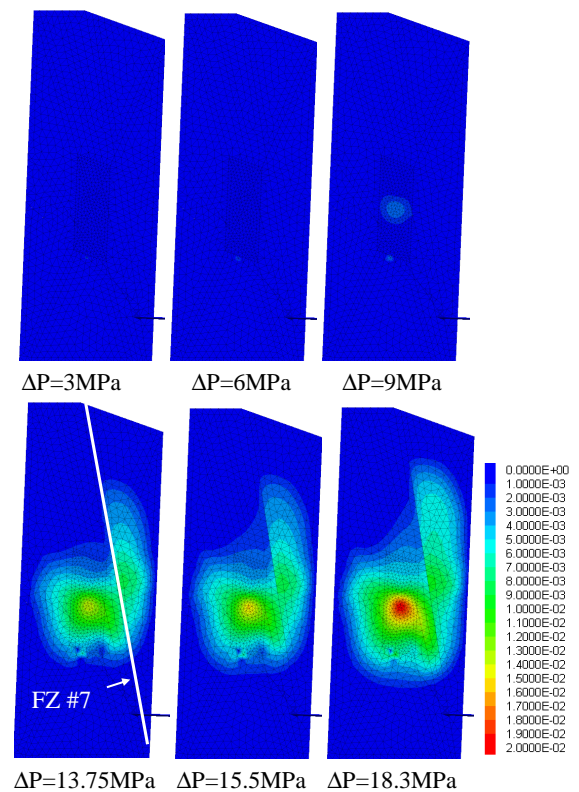

ΔP=3MPa   ΔP=6MPa   ΔP=9MPa

FZ #7

ΔP=13.75MPa   ΔP=15.5MPa   ΔP=18.3MPa

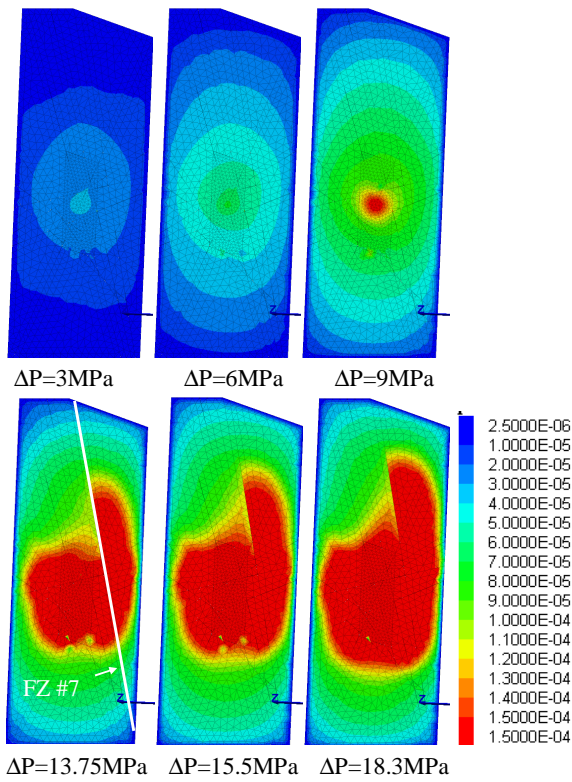**Figure 6: GPK4 - Shear displacement contours [m] in fault zone #8, for each overpressure stage ΔP**

Figure 7: GPK4 – Hydraulic aperture contours [m] in fault zone #8, for each overpressure stage ΔP

The shear displacement contours in fault zone #7 is shown in Figure 8, cut by the fault zones #2, #5 and #8. The shape of the shear displacement contours is not centered on the injection well and depends on the intersection between fault zone #7 and the other fault zones.
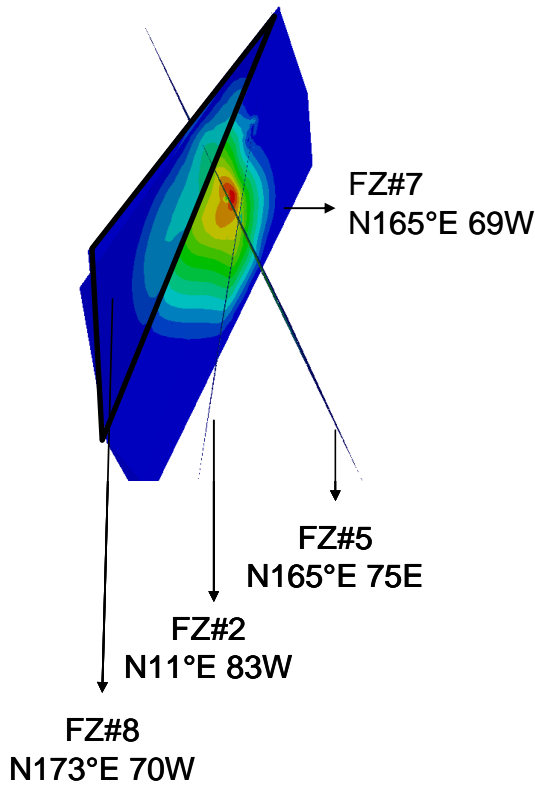

Figure 8: GPK4 – Perspective view of the shear displacement contours [m] in fault zones #2, #5, #7 and #8 at overpressure stage ΔP = 18.3 MPa

3.2 GPK4 Well-Shutdown Modelling

Once the stimulation test is performed, the well is shut down by applying a zero flowrate at the wellhead. In order to avoid any numerical instability, the null flowrate is not applied instantaneously, but is applied with a decreasing ramp, during which some fluid is still injected into the well. This does not correspond exactly to the in-situ adopted well shutdown procedure, in which the well is either shut down almost instantaneously by shutting down the pump, or it is shut down by applying decreasing overpressure stages.

Figure 9 and 10 display the shear displacement contours and the hydraulic aperture contours at the end of the stimulation test (18.3 MPa overpressure) and after well-shut down (0 MPa overpressure), respectively, in fault zone plane #8 (striking N173°E), fault zone plane #6 (striking N147°E), and fault zone plane #1 (striking N4°E).

For fault zone #8, which is favorably oriented in relation to the stress state so that it shears, the shear displacements still increase slightly as the well is being shut down. This could be due to the well shutdown mode described above, during which a certain amount of fluid is injected. A large surface in fault zone #8 has a hydraulic aperture 50 times greater than the hydraulic aperture it had before the stimulation. This large hydraulic aperture that remains after the well has been shut down proves that the hydraulic stimulation test creates irreversible permeability. As seen earlier, this creation is due to the shearing in the fault zone plane. The same observation can be made for the fault zones #2, #5, and #7, which sheared during the hydraulic stimulation test.
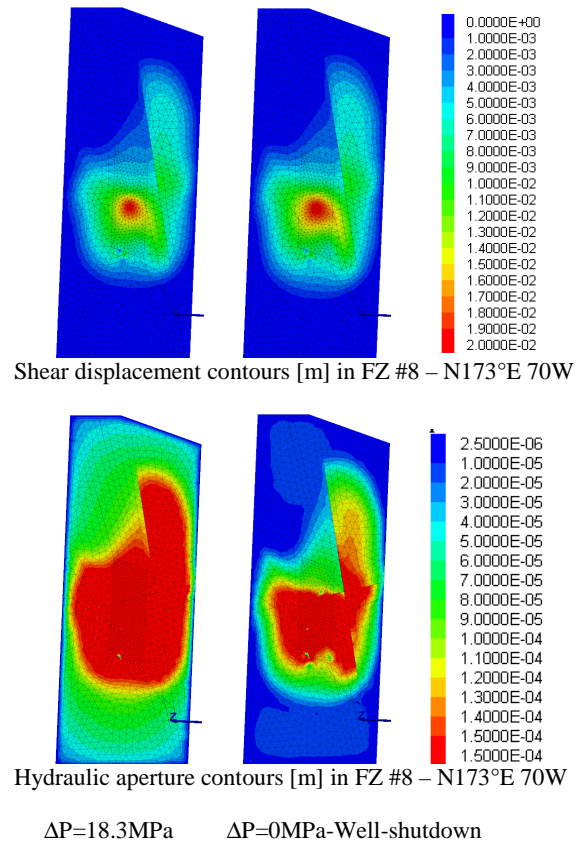

Shear displacement contours [m] in FZ #8 – N173°E 70W

Hydraulic aperture contours [m] in FZ #8 – N173°E 70W

ΔP=18.3MPa   ΔP=0MPa-Well-shutdown

Figure 9: GPK4 - Shear displacement contours [m] and Hydraulic aperture contours [m] in fault zone #8 N173°E 70W before and after well-shutdown

Shear displacement contours [m] in FZ #6 – N147°E 66W

Hydraulic aperture contours [m] in FZ #6 – N147°E 66W
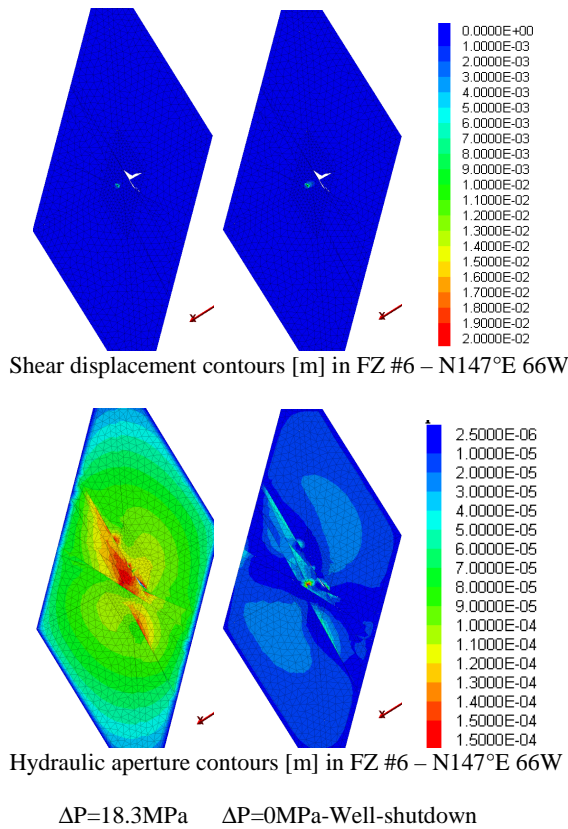
ΔP=18.3MPa   ΔP=0MPa-Well-shutdown

Figure 10: GPK4 - Shear displacement contours [m] and Hydraulic aperture contours [m] in fault zone #6 N147°E 66E before and after well-shutdown

Shear displacement contours [m] in FZ #1 – N4°E 86W

Hydraulic aperture contours [m] in FZ #1 – N4°E 86W

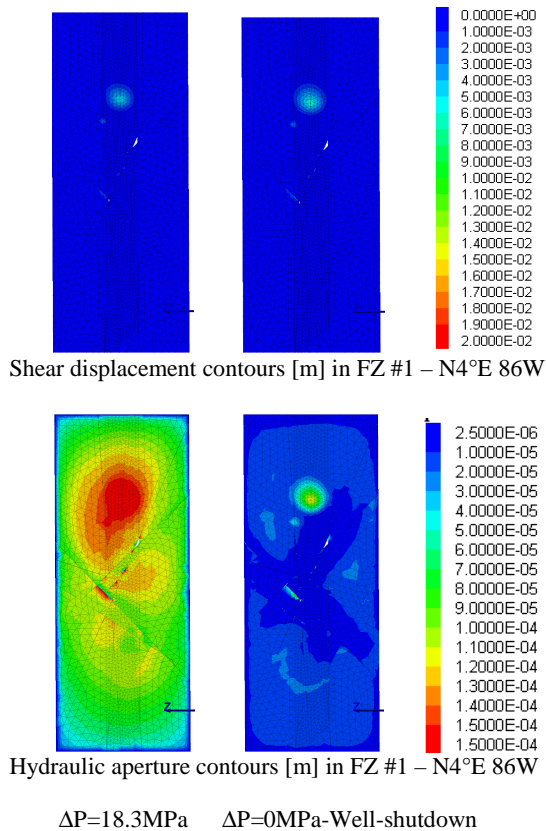ΔP=18.3MPa   ΔP=0MPa-Well-shutdown

Figure 11: GPK4 - Shear displacement contours [m] and Hydraulic aperture contours [m] in fault zone #1 N4°E 86W before and after well-shutdown

The permeable fault zone #6 does not shear during the hydraulic stimulation test like the other permeable fault zones. The shape of the shear displacement contours at the end of the stimulation test and after the well is shut down exhibit less than 1 mm shearing. However, once the well is shut down, there are still more hydraulic apertures than before the well was stimulated. The shape of the remaining hydraulic aperture is determined by the intersection between fault zone #6 and the other fault zones. The resulting irreversible permeability increase in this fault zone is strongly anisotropic.

For fault zone #1, which is not favorably oriented in relation to the stress state for shearing, only little shear displacement of about 5 mm occurs and is restricted to a surface area of about a 5-10 m radius circle centered on the well. Once the well is shut down, some hydraulic apertures remained in a small area with a radius of about 20 m around the well (about 10 times the initial hydraulic apertures). The rest of the fault zone plane has a hydraulic aperture close to the initial hydraulic aperture before the well was stimulated.

3.3 GPK4 Post-Stimulation Injection Test Modelling

Once the well is shut down, a post-stimulation injection test is performed by applying increasing overpressure stages at the wellhead (3, 6, 9, 12 and 15 MPa).

Plots of pressure at the wellhead vs. the total injected flowrate during the stimulation test and during the post-stimulation injection test are shown in Figure 12. For the 6 MPa overpressure stage, the total injected flowrate into the well is about 10 times greater than the flowrate injected during the stimulation test. This clearly shows that the hydraulic stimulation test created an irreversible permeability increase, as the pressure-flowrate curve obtained for the post-stimulation injection test is below the curve obtained for the stimulation test.

For greater overpressure stages, the pressures-flowrate curve obtained during the post-stimulation injection test began to approach the curve obtained during the stimulation injection test. The irreversible permeability increase is not linear with respect to the applied overpressure.
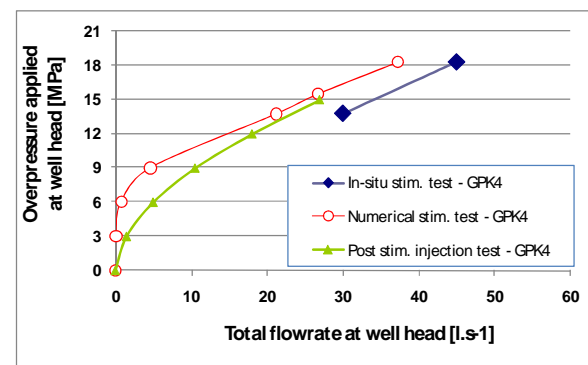

Figure 12: GPK4 – Pressure vs. total flowrate at the wellhead during stimulation test and post-stimulation injection test

CONCLUSION AND DISCUSSION

The adopted numerical approach successfully simulated the behavior of a fractured rock mass during hydraulic stimulations of a deep well and post-stimulation injection tests after the well was shut down. The modelling of the post-stimulation injection test applied to GPK4 confirms the irreversible permeability increase, which is due to existing

data of previous stimulations in these fault zones. This permeability increase could be due to the shearing that occurs in the fault zones during the hydraulic stimulation tests.

The tangential mechanical constitutive law used for the fault zones was the Mohr-Coulomb slip model with dilation effect. With respect to this constitutive law, the fault zone opening is proportional to its shear displacement. Another constitutive law is currently being used, which accounts for fault zone damage associated to the shearing. With such a constitutive law, the dilation effect is not simply proportional to the shear displacement; it depends on the joint roughness and accounts for asperity breakage. This constitutive law should allow the reproduction of significant irreversible permeability increases.

This information gained with this approach should allow in the introduction of a flow model of the reservoir (Gentier et al, 2009) zones where the permeability was increased by the stimulations.

ACKNOWLEDGEMENTS

REFERENCES

3DEC (2008), Version 4.0, 3 Dimensional Distinct Element Code. User's Manual. Itasca Consulting Group Inc., Minneapolis, MN., June 2008.

Cornet, F.H., Bérard, Th., Bourouis, S. (2007), How close to failure is a granite rock at a 5km depth?, Int. J. Rock Mech. & Min. Sci., Vol. 44, pp47-66, July 2007.

Gentier, S., Hosni, A., Rachez, X., et al. (2004) – Projet GEFRAC (module 1) Modélisation du comportement hydro-thermo-mécanique des milieux fracturés – Rapport final. BRGM/RP-53528-FR, 259 p.

Gentier, S., Dezayes, C., Rachez, X., et al. (2005) - Thermo-Hydro-Mechanical modelling of the deep geothermal wells at Soultz-sous-Forêts. Proceedings of the European Hot Dry Rock Association Scientific Conference, March 2005.

Gentier, S. et al. (2008). Projet GEFRAC 2 (module1) : Recherche en appui au développement des ressources géothermiques en milieux fracturés – Modèles de comportement thermo-hydro-mécanique. Rapport final BRGM/RP-56704-FR, 218p.

Gentier, S. Rachez, X., Trans Ngoc, T. D., Peter-Borie, M, Souque, C. (2009) – 3D flow modelling of the medium-term circulation test performed in the deep geothermal site of Soultz-sous-Forêts (France). In Proceedings World Geothermal Congress 2010, Bali, Indonesia, 25-29 April 2010.

Rachez X., Gentier S, Blaisonneau A. (2006) – Hydro-Mechanical behavior of GPK3 and GPK4 during the hydraulic stimulation test – Influence of the stress field. Proceedings of the European Hot Dry Rock Association Scientific Conference, June 2006.